

Wave Turbulence in Self-Gravitating Bose Gases

Jonathan Skipp

Centre for Complexity Science, University of Warwick, Coventry CV4 7AL, UK

Victor L'vov

Department of Chemical and Biological Physics, Weizmann Institute of Science, Rehovot 76100, Israel

Sergey Nazarenko

Université Côte d'Azur, CNRS, Institut de Physique de Nice, Parc Valrose, 06108 Nice, France

We develop the theory of weak wave turbulence in systems described by the Schrödinger-Helmholtz equation in two and three dimensions. This model contains as limits both the familiar cubic nonlinear Schrödinger equation, and the Schrödinger-Newton equations, the latter being a nonrelativistic model of Fuzzy Dark Matter which has a nonlocal gravitational self-potential. We show that in the weakly-nonlinear limit the Schrödinger-Helmholtz equation has a simultaneous inverse cascade of particles and a forward cascade of energy. The inverse cascade we interpret as a nonequilibrium condensation process, which could be a precursor to collapses and structure formation at large scales (for example the formation of galactic dark matter haloes). We show that for the Schrödinger-Newton equation in two and three dimensions, and in the two-dimensional nonlinear Schrödinger equation, the particle and energy fluxes are carried by small deviations from thermodynamic distributions, rather than the Kolmogorov-Zakharov cascades that are familiar in wave turbulence. We develop a differential approximation model to characterise such “warm cascade” states.

I. INTRODUCTION

A. Wave turbulence cascades

The dynamical and statistical behaviour of random weakly-interacting waves is responsible for many important physical effects across applications ranging from quantum to classical and to astrophysical scales [1, 2]. Assuming weak nonlinearity and random phases, such behaviour is described by the theory of weak wave turbulence [1, 2]. As in the theory of classical hydrodynamic turbulence, weak wave turbulence theory can predict nonequilibrium statistical states characterised by cascades of energy and/or other invariants through scales. Sometimes, similarly to 2D classical turbulence, such cascades are dual, with one invariant cascading to smaller scales (direct cascade) and the other invariant toward the large scales (inverse cascade). An inverse cascade often leads to accumulation of the turbulence spectrum near the largest scale of the system, which is analogous to Bose-Einstein condensation. Large-scale coherent structures may form out of such a condensate and further evolve via mutual interactions and interactions with the background of random waves, thereby realising a scenario of order emerging from chaos.

In the present paper, we will study a precursor to such a process of coherent structure formation by developing the wave turbulence theory and describing the dual cascade in the so-called “Schrödinger-Helmholtz equations” that arise in cosmological and nonlinear optics applications.

B. Schrödinger-Helmholtz equations

The Schrödinger-Helmholtz equations are the nonlinear partial differential equations

$$i\partial_t\psi + \nabla^2\psi - V[\psi]\psi = 0, \quad (1a)$$

$$\nabla^2V - \Lambda V = \gamma|\psi|^2 \quad (1b)$$

for a complex scalar field $\psi(\mathbf{x}, t)$ in which $V[\psi]$ plays the role of (potential) interaction energy and Λ and γ are dimensionless constants. We will be interested in systems set in two and three spatial dimensions (2D and 3D, respectively).

Before proceeding in the body of the paper with developing the statistical description of the nonlinear field ψ in the framework of Eqs. (1), we will first outline in this Sec. I B the important physical contexts in which Eqs. (1) have been used, the previous results found, and the findings that we anticipate will arise from our approach.

Notice that depending on the spatial scale of interest ℓ , one term or the other on the left-hand side of Eq. (1b) is dominant. For $\ell \gg \ell_* = 2\pi/\sqrt{\Lambda}$ the Schrödinger-Helmholtz equations (1) become the more familiar cubic nonlinear Schrödinger equation, discussed in Sec. I B 1, while for $\ell \ll \ell_*$ they turn into the Schrödinger-Newton equations, see Sec. I B 2. Finally, in Sec. I B 3 we return to interpret the Schrödinger-Helmholtz Eqs. (1) in light of the discussion of these limits.

1. Large-scale limit: the nonlinear Schrödinger equation

In the limit of large scales, $\ell \gg \ell_*$, the first term on the left-hand side of Eq. (1b) can be neglected and one

immediately finds that $V[\psi] = -(\gamma/\Lambda)|\psi|^2$. The constant γ/Λ can be removed by proper renormalization of $|\psi|^2$, leaving only the sign of this constant, denoted as $s = \pm 1$. Thus the Schrödinger-Helmholtz Eqs. (1) become the nonlinear Schrödinger equation

$$i\partial_t\psi + \nabla^2\psi + s|\psi|^2\psi = 0, \quad (2)$$

also known as the Gross-Pitaevskii equation [3]. This equation has a cubic, spatially local, attractive (for $s = +1$) or repulsive (for $s = -1$) interaction.

The nonlinear Schrödinger Eq. (2) is well-known in the study of Bose-Einstein condensates [3], where ψ is the wavefunction of a system of identical bosons in the Hartree-Fock approximation [4, 5] and the nonlinearity is due to s-wave scattering.

Equation (2) is also familiar in the field of nonlinear optics [6] when a light beam, whose electric field is slowly modulated by an envelope ψ (such that its intensity is $|\psi|^2$), impinges on a dispersive, nonlinear medium, inducing a nonlinear change in the medium's refractive index via the Kerr effect. Equation (2) then describes the evolution of the beam's envelope in the paraxial approximation, where t becomes the length along the beam axis, and the remaining spatial directions are transverse to the beam. In this context s is the normalised Kerr coefficient and the cases with $s = +1/-1$ are known as the focusing/defocusing nonlinear Schrödinger equation respectively, terminology that we adopt here in the general case.

The nonlinear Schrödinger Eq. (2) is studied in a great many other systems due to its universality in describing the slowly-varying envelope of a monochromatic wave in a weakly nonlinear medium [7]. We shall not pursue its other applications in this work, instead merely noting that due to its universality many monographs and papers have been dedicated to the study of Eqs. (2) and its solutions.

2. Small-scale limit: the Schrödinger-Newton equations

Now we focus on scales $\ell \ll \ell_*$, when the second term in the left-hand side of Eq. (1b) dominates. Then the Schrödinger-Helmholtz Eqs. (1) simplify to the coupled equations

$$i\partial_t\psi + \nabla^2\psi - V[\psi]\psi = 0, \quad (3a)$$

$$\nabla^2 V = \gamma|\psi|^2. \quad (3b)$$

If we retain the interpretation of $\psi(\mathbf{x}, t)$ as a boson wavefunction, we see that the nonlinearity in Eq. (3a) is nonlocal, coming from an extended potential $V[\psi]$ that solves the Poisson Eq. (3b) for which the source is proportional to the boson number density $\rho = |\psi|^2$. Specifying $\gamma = 4\pi Gm$, with m the boson mass and G Newton's gravitational constant, we observe that Eqs. (3) describe a dilute Bose gas moving at nonrelativistic speeds under

the influence of a Newtonian gravitational potential generated by the bosons themselves. It is for this reason that Eqs. (3) are known as the Schrödinger-Newton equations.

The use of Eqs. (3) to represent self-gravitating Bose gases in the Newtonian limit is important in cosmology, where they are used to model “fuzzy dark matter”. This is the hypothesis that dark matter is comprised of ultralight ($m \lesssim 1 \times 10^{-22}$ eV) scalar bosons whose de Broglie wavelengths are on the order of galaxies ($\lambda_{\text{dB}} \sim 1$ kpc) [8–11]. In this scenario galactic dark matter haloes are gigantic condensates of this fundamental boson, trapped by their own gravity and supported by quantum pressure arising from the uncertainty principle [8, 12–14].

Fuzzy dark matter is an alternative to the standard model of cosmology which supposes that dark matter is comprised of thermal but sub-luminal, weakly interacting massive particles, i.e. “cold dark matter” [15]. While cold dark matter is successful at describing the observed large-scale structure of the Universe, its accelerated expansion, and the fluctuations of the cosmic microwave background [16, 17], at small scales it fails to reconcile observations with cosmological simulations, particularly in matching the inferred flat density profiles of galactic dark matter haloes with the cuspy profiles found in simulations, and the lack of observed satellite dwarf galaxies as compared to theoretical predictions [18, 19]. By contrast, in fuzzy dark matter structures on the order of λ_{dB} are suppressed by the uncertainty principle [8, 20] and, when included in the model, s-wave scattering¹ [10, 13, 21], providing a resolution to the small-scale problems of cold dark matter. At large scales the two models become indistinguishable [20]. Thus, until the precise nature of dark matter particles is identified, fuzzy dark matter must be considered alongside cold dark matter when investigating the formation of large-scale structure in the early Universe [20, 22–24].

Like the nonlinear Schrödinger Eq. (2), the Schrödinger-Newton Eqs. (3) also find application in nonlinear optics. Again (3a) is the equation for the envelope of the beam, however (3b) expresses a nonlocal change in refractive index due to the incident beam energy diffusing as heat through the nonlinear medium [25–27]: the thermo-optic effect. Of course optical experiments are constrained to the one or two spatial dimensions transverse to the beam, whereas astrophysics takes place in three dimensions. However the Schrödinger-Newton Eqs. (3) are a quantitative

¹ Note that we only consider the gravitational nonlinearity in (3b). Including local scattering would result in an extra term, c.f. the cubic term in Eq. (2). As we have mentioned, our focus in this work is the turbulent behaviour of Eqs. (1) and their limits. Much is already known about the turbulence of Eq. (2), so in order to concentrate on the features that arise from coupling the boson field to gravity, we restrict our attention to the nonlocal gravitational nonlinearity in Eq. (3b), corresponding to gravitational effects greatly outweighing boson self-interaction.

nonlinear model that describes both tabletop optics experiments and the physics of galaxies and clusters, and indeed recent optics experiments have elucidated interesting nonlinear effects that have been interpreted in the astrophysical context [27, 28]. Results in two dimensions may also be relevant to astrophysics as fuzzy dark matter simulations suggest that cosmological structures develop from random fluctuations into quasi-cylindrical filaments before collapsing into spherical structures [23, 24].

It is precisely the dynamical formation of the largest scale structure, the precursor to filaments and haloes, that we wish to examine in this work. Thus after returning briefly to the Schrödinger-Helmholtz Eqs. (1) we will turn to the question of turbulence, and recap what is known about the turbulent formation of structure in nonlinear Schrödinger type models.

3. Physical applications of the Schrödinger-Helmholtz equations

The Schrödinger-Helmholtz Eqs. (1), then, are a model that captures the physics present in both Eq. (2) and Eqs. (3). In the optical context they model a system where both the thermo-optic and the Kerr effects are important [29–31]. Alternatively, the diffusion term in Eq. (1b) can appear due to heat losses at the experimental boundaries of an optical sample [27]. Thus the Schrödinger-Helmholtz equations are a model that has wide applicability in the analysis of optical systems where the nonlinearity has both local and nonlocal contributions.

Applied to fuzzy dark matter the local term in Eq. (1b) corresponds to the inclusion of a cosmological constant Λ in the Newtonian approximation of the Einstein field equations [32]. This is necessary if one wants to account for a dark energy component to cosmology in a Newtonian approximation. It is also a means to regularise the so-called “Jeans swindle”—the specification that Eq. (3b) only relates the fluctuations of density and potential around an unspecified equilibrium [33]. To elaborate, Eq. (3b) is well-posed for spatially infinite domains in which the support of $\rho(\mathbf{x}) = |\psi(\mathbf{x})|^2$ is compact, but if one seeks an equilibrium with spatially-constant V and ρ the only solution is the trivial null solution (an empty domain). The Jeans swindle is the *ad hoc* replacement of V in Eq. (3a) with \tilde{V} that solves $\nabla^2 \tilde{V} = \gamma \tilde{\rho}$, where the tildes refer to fluctuations of quantities about a nonzero equilibrium, whose existence is entirely paradoxical. In a periodic domain $\Omega = \mathbb{T}_L^d$ of side L the equivalent problem is that Eq. (3b) can only be satisfied when Ω is empty, as can be seen by integrating over Ω , and using the divergence theorem and the periodic boundary conditions. The Jeans swindle is then implemented by replacing (3b) with

$$\nabla^2 \tilde{V} = \gamma (\rho - \langle \rho \rangle_\Omega) \quad (4)$$

where the box average of the number density $\langle \rho \rangle_\Omega = L^{-d} \int_\Omega \rho d\mathbf{x}$ is the equilibrium solution, and one solves only for \tilde{V} .

It is shown in Ref. [32] in the infinite-domain case that the Jeans swindle can formally be justified by considering the Helmholtz-like Eq. (1b) instead of Eq. (3b), as the former is well-posed without the restriction of the right-hand side needing to integrate to zero, and then taking the limit $\Lambda \rightarrow 0$. For the case of the periodic boundary we simply note that averaging (1b) gives $\langle V \rangle_\Omega = -\langle \rho \rangle_\Omega / \Lambda$. Substitution back into (1b) and writing $V = \tilde{V} + \langle V \rangle_\Omega$ recovers Eq. (4) in the limit $\Lambda \rightarrow 0$.

We therefore take the Schrödinger-Helmholtz Eqs. (1), as our model of interest as they comprise a physically relevant model that is useful in both astrophysics and nonlinear optics. It contains as limits both the nonlinear Schrödinger equation, about which much is known, and the Schrödinger-Newton equation, whose relevance is starting to come to the fore. Next we discuss weak and strong turbulence in these latter models, and introduce the process that is a precursor to the formation of large structures.

C. Turbulence in the nonlinear Schrödinger and Schrödinger-Newton equations

Turbulence in laboratory Bose-Einstein condensates [34–36] and optics [31, 37, 38] is now a well-established field, and much has been understood by using the cubic nonlinear Schrödinger Eq. (2). Its dynamics is rich, with weakly nonlinear waves typically coexisting with coherent, strongly nonlinear structures. The nature of these structures depends radically on the sign of interaction term s in Eq. (2). In the defocusing (repulsive) case they include stable condensates: accumulations of particles (in the Bose-Einstein condensate case) or intensity (optics) at the largest scale, with turbulence manifesting as a collection of vortices in 2D, or a tangle of vortex lines in 3D, on which the density is zero and which carry all the circulation, propagating through the condensate [2, 36]. In the focusing (attractive) case solitons and condensates are unstable above a certain density, with localised regions of over-density collapsing and becoming singular in finite time [37, 39].

On the other hand, turbulence in the Schrödinger-Newton Eqs. (3) have only recently been investigated by direct numerical simulation in the cosmological setting [22] and appears to contain features of both the focusing and the defocusing nonlinear Schrödinger equation. As mentioned above, at large scales the Schrödinger-Newton model exhibits gravitationally-driven accretion into filaments which then become unstable and collapse into spherical haloes [23, 24] (c.f. collapses in the focusing nonlinear Schrödinger model driven by the self-focusing local contact potential). However within haloes the condensate is stable, with turbulence in an envelope surrounding the core manifesting

as a dynamic tangle of reconnecting vortex lines, as in the defocusing nonlinear Schrödinger model [22]. This is to be expected, given that the attractive feature of the Schrödinger-Newton model in cosmology is that it is simultaneously unstable to gravitational collapse and stable once those collapse event have regularised into long-lived structures, and so it should contain features of both the unstable (focusing) and stable (defocusing) versions of the nonlinear Schrödinger model.

To understand more fully the phenomenology recently reported in the Schrödinger-Newton Eqs. (3), it is tempting to apply theoretical frameworks that have been successful in explaining various aspects of turbulence in the nonlinear Schrödinger equation. One such theory is wave turbulence: the study of random broadband statistical ensembles of weakly interacting waves [1, 2]. The “turbulent” behaviour referred to here is the statistically steady-state condition where dynamically conserved quantities cascade through scales in the system via the interaction of waves, a process analogous to the transfer of energy in 3D classical fluid turbulence (and respectively energy and enstrophy in 2D.) Wave-turbulence theory is integral to the quantitative description of both the wave component and the evolution of the coherent components of the nonlinear Schrödinger system and is relevant in three regimes: Bogoliubov sound waves on the background of a strong condensate [2, 37], Kelvin waves that are excited on quantized vortex lines in a condensate [2, 40], and de Broglie waves propagating in the absence of a condensate [2, 37]. In the latter case the theory of wave turbulence describes how, starting from a random ensemble of waves, a dual turbulent cascade simultaneously builds up the large-scale condensate while sending energy to small scales [2]. As we will describe in section II C below, this dual cascade is generic in any system of interacting waves with two quadratic dynamical invariants (particles and energy in the cases of interest here). The theory of wave turbulence thus provides a universal description of how large-scale coherent structures can arise from a random background.

D. Organisation of this paper

In this work, then, we develop the theory of wave turbulence for the Schrödinger-Helmholtz Eqs. (1) in the case of fluctuations about a zero background. By taking the limits of small and large Λ we obtain the wave turbulence of the Schrödinger-Newton Eqs. (3) and also review known results of the nonlinear Schrödinger Eq. (2). Our aim is to describe the first stages of evolution from random waves to the dynamical formation of a large-scale condensate in cosmology and in nonlinear optics. From this structure gravitational-type collapses will ensue and the phenomenology described above will develop.

In Secs. II A and II B we overview the wave turbulence theory and arrive at the wave kinetic equation that describes the evolution of the wave content of the sys-

tem. Section II C describes the dual cascade of energy towards small scales and particles towards large scales in the system. In Secs. II D and II E we describe respectively the scale-free pure-flux spectra that are formal stationary solutions of the wave kinetic equation. However in Sec. II F we show that these stationary spectra yield the wrong directions for the fluxes of energy and particles, as compared with the directions predicted in Sec. II C. We resolve this paradox by developing a reduced model of the wave dynamics in Secs. II G and II H and using it in Sec. III to reveal the nature of the dual cascades in the nonlinear Schrödinger and the Schrödinger-Newton limits of the Schrödinger-Helmholtz equation. We conclude in Sec. IV and suggest further directions of research incorporating wave turbulence into the study of the Schrödinger-Helmholtz equation.

II. BUILDING BLOCKS OF SCHRÖDINGER-HELMHOLTZ WAVE TURBULENCE

In this Section we overview the aspects of the wave turbulence theory that we require in our description of turbulence in the Schrödinger-Helmholtz model.

A. Hamiltonian formulation of the Schrödinger-Helmholtz equations

To put the Schrödinger-Helmholtz turbulence in the context of general theory of wave turbulence we need to formulate Schrödinger-Helmholtz Eqs. (1) in the Hamiltonian form. For that goal we first set the system in the periodic box $\Omega = \mathbb{T}_L^d$ and decompose variables into Fourier modes

$$\psi_{\mathbf{k}}(t) = L^{-d} \int_{\Omega} \psi(\mathbf{x}, t) \exp[-i(\mathbf{k} \cdot \mathbf{x} - \omega t)] d\mathbf{x},$$

and similarly for $V_{\mathbf{k}}(t)$. The dynamical equations become

$$i\partial_t \psi_{\mathbf{k}} - k^2 \psi_{\mathbf{k}} - \sum_{1,2} V_1 \psi_2 \delta_{12}^{\mathbf{k}} = 0, \quad (5a)$$

$$-(k_1^2 + \Lambda)V_1 = \gamma \sum_{3,4} \psi_3 \psi_4^* \delta_{14}^3, \quad (5b)$$

where $V_j = V_{\mathbf{k}_j}$, $\psi_j = \psi_{\mathbf{k}_j}$, $\sum_{i\dots j} = \sum_{\mathbf{k}_i, \dots, \mathbf{k}_j}$ and $\delta_{12}^{\mathbf{k}} = \delta(\mathbf{k} - \mathbf{k}_1 - \mathbf{k}_2)$ is the Kronecker delta, equal to unity if $\mathbf{k} = \mathbf{k}_1 + \mathbf{k}_2$ and zero otherwise².

² If we start with Eq. (3b), i.e. $\Lambda = 0$, from the outset, then we need to set $V_0 = 0$, which is the Jeans swindle in Fourier space. This corresponds to subtraction of the mean as in Eq. (4), i.e. $\langle \rho \rangle_{\Omega} = 0$.

Eqs. (5) can be rewritten as the canonical Hamiltonian equation

$$i\partial_t\psi_{\mathbf{k}} = \frac{\partial H}{\partial\psi_{\mathbf{k}}^*}, \quad H = H_2 + H_4, \quad (6a)$$

$$H_2 = \sum_{\mathbf{k}} \omega_{\mathbf{k}} \psi_{\mathbf{k}} \psi_{\mathbf{k}}^*, \quad (6b)$$

$$H_4 = -\frac{1}{2} \sum_{1234} W_{34}^{12} \psi_1 \psi_2 \psi_3^* \psi_4^* \delta_{34}^{12}. \quad (6c)$$

Here the Hamiltonian H is comprised of the quadratic part H_2 , which leads to linear waves with dispersion relation $\omega_{\mathbf{k}} = k^2$, and the interaction Hamiltonian H_4 which describes 4-wave coupling of the $2 \leftrightarrow 2$ type. The interaction coefficient W_{34}^{12} can be written in the symmetric form

$$W_{34}^{12} = \frac{\gamma}{4} (A_{1234} + A_{2134} + A_{1243} + A_{2143}), \quad (6d)$$

$$A_{1234} = 1 / [(\mathbf{k}_1 - \mathbf{k}_4) \cdot (\mathbf{k}_3 - \mathbf{k}_2) + \Lambda]. \quad (6e)$$

If we are using the Jeans swindle from the outset (see Footnote 2) then the sum in Eq. (6c) must exclude all terms when any two wavenumbers are equal.

For completeness, we note that if we include a local cubic self-interaction term $-s|\psi|^2\psi$ on the right-hand side of Eq. (3a) as well as the gravitational term then the 4-wave interaction coefficient would be

$$W_{34}^{12} = -s + \frac{\gamma}{4} (A_{1234} + A_{2134} + A_{1243} + A_{2143}) \quad (6f)$$

with A_{1234} as in Eq. (6e). Finally, the 4-wave interaction coefficient for the cubic nonlinear Schrödinger Eq. (2) is simply

$$W_{34}^{12} = -s.$$

B. Kinetic equation and conserved quantities

In the theory of weak wave turbulence we consider ensembles of weakly interacting waves with random phases uniformly distributed in $[0, 2\pi)$, and independently-distributed amplitudes [2, 41–43]. We define the wave spectrum

$$n_{\mathbf{k}} = (L/2\pi)^d \langle |\psi_{\mathbf{k}}|^2 \rangle, \quad (7)$$

where the angle brackets $\langle \dots \rangle$ denote averaging of “...” over the random phases and amplitudes.

In the limit of an infinite domain $L \rightarrow \infty$ and for weak nonlinearity $|H_4/H_2| \ll 1$ one can derive [1, 2, 37] a wave kinetic equation for the evolution of the spectrum. For $2 \leftrightarrow 2$ wave processes with the interaction Hamiltonian as in Eq. (6c), the kinetic equation is

$$\begin{aligned} \partial_t n_{\mathbf{k}} = & 4\pi \int |W_{3\mathbf{k}}^{12}|^2 \delta_{3\mathbf{k}}^{12} \delta(\omega_{3\mathbf{k}}^{12}) n_1 n_2 n_3 n_{\mathbf{k}} \\ & \times \left[\frac{1}{n_{\mathbf{k}}} + \frac{1}{n_3} - \frac{1}{n_1} - \frac{1}{n_2} \right] d\mathbf{k}_1 d\mathbf{k}_2 d\mathbf{k}_3, \end{aligned} \quad (8)$$

where $\delta_{3\mathbf{k}}^{12}$ is now a Dirac delta function that imposes wavenumber resonance $\mathbf{k} + \mathbf{k}_3 = \mathbf{k}_1 + \mathbf{k}_2$; likewise frequency resonance $\omega_{\mathbf{k}} + \omega_3 = \omega_1 + \omega_2$ is enforced by the Dirac delta $\delta(\omega_{3\mathbf{k}}^{12})$.

The kinetic equation (8) describes the irreversible evolution of an initial wave spectrum via 4-wave interaction³. As the spectrum evolves the following two quantities are conserved by the kinetic equation

$$N = \int n_{\mathbf{k}} d\mathbf{k}, \quad (9a)$$

$$E = \int \omega_{\mathbf{k}} n_{\mathbf{k}} d\mathbf{k}. \quad (9b)$$

Here N is known as the (density of) waveaction, or particle number, and is conserved for all times by the original Eqs. (1), and E is referred to as the (density of) energy. It is the leading-order part of the total Hamiltonian, i.e. H_2 , and is only conserved by Eqs. (1) over timescales for which the kinetic equation (8) is valid.

For isotropic systems such as Eqs. (1) we can express the conservation of invariants (9) as scalar continuity equations for the waveaction

$$\partial_t N_k^{(1D)} + \partial_k \eta = 0, \quad N_k^{(1D)} = \mathbb{A}^{(d-1)} n_{\mathbf{k}} k^{d-1}, \quad (10a)$$

and for the energy

$$\partial_t E_k^{(1D)} + \partial_k \epsilon = 0, \quad E_k^{(1D)} = \omega_{\mathbf{k}} N_k^{(1D)}. \quad (10b)$$

Here $\eta = \eta(k)$ and $\epsilon = \epsilon(k)$ are, respectively, the flux of waveaction and energy through the shell in Fourier space of radius $k = |\mathbf{k}|$. In Eq. (10a) we have defined the isotropic 1-dimensional (1D) waveaction spectrum $N_k^{(1D)}$, where $\mathbb{A}^{(d-1)}$ is the area of a unit $(d-1)$ -sphere; likewise in Eq. (10b) $E_k^{(1D)}$ is the isotropic 1D energy spectrum.

In the rest of this work we will consider a forced-dissipated system, with forcing in a narrow band at some scale k_f and dissipation at the large and small scales k_{\min} and k_{\max} respectively, and that these scales are widely separated $k_{\min} \ll k_f \ll k_{\max}$. The interval $k_f < k < k_{\max}$ is known as the direct inertial range, and the $k_{\min} < k < k_f$ is called the inverse inertial range, because of the directions that E and N flow through these ranges, as we describe in the next Section. In this open setup the local conservation Eqs. (10) will hold deep inside the inertial ranges but the global quantities N and E are only conserved if the rates at which they are injected match their dissipation rates.

³ Note that the interaction coefficient enters Eq. (8) only through its squared modulus, meaning that the sign of the interaction does not play a role in the weakly nonlinear limit. This means that, for example, in the case of Eq. (2) the buildup of a large-scale condensate via an inverse cascade is the same for both the focusing and defocusing case, and the difference only enters in the strongly nonlinear evolution.

We examine the open system because it allows the nonequilibrium stationary solutions Eq. (8) to form, allowing us to examine the dual cascade in its purest manifestation. Alternatively one could study a situation where turbulence evolves freely from an initial condition. In this case analytical progress can be made by studying self-similar temporal solutions to the kinetic equation that either fill out the inertial range in a finite time, or take an infinite time to develop [44–46]. This is a topic to explore in future work.

C. Fjørtoft argument for two conserved invariants

The presence of two dynamical invariants E and N whose densities differ by a monotonic factor of k , here by $\omega_{\mathbf{k}} = k^2$, places strong constraints on the directions in which the invariants flow through \mathbf{k} -space, as pointed out by Fjørtoft [47]. We recapitulate his argument in its open-system form⁴.

Consider the system in a steady state where forcing balances dissipation: at k_f energy and particles are injected at rate ϵ and η respectively, and dissipated at those rates at k_{\min} or k_{\max} . The ratio of the density of energy to the density of particles is k^2 , and so the energy and particle flux must be related by the same factor at all scales. At the forcing scale this means that $\epsilon \sim k_f^2 \eta$.

The argument proceeds by contradiction. Suppose that the energy is dissipated at the large scale k_{\min} at the rate $\sim \epsilon$ that it is injected. Then at this scale particles would be removed at rate $\sim \epsilon/k_{\min}^2 \sim \eta k_f^2/k_{\min}^2 \gg \eta$ which is impossible because then the dissipation would exceed the forcing. Therefore in a steady state most of the energy must be dissipated at small scales k_{\max} . Likewise, if we assume the particles are removed at the small scale k_{\max} at rate $\sim \eta$ then energy would be removed at the impossible rate $\sim \epsilon k_{\max}^2/k_f^2 \gg \epsilon$ so most of the particles must be removed at large scales k_{\min} instead.

Therefore this argument predicts that the scale containing most of the energy must move towards high k while the scale containing the most particles must move towards low k . Particles are then removed if k_{\min} represents a dissipation scale. However if there is no dissipation here then the spectrum develops a localised bump as the particles accumulate at the largest scale—this is the condensate. In this case k_{\min} represents the transition scale between the condensate, which becomes strongly nonlinear as the dual cascade proceeds, and the weakly nonlinear wave component of the system which continues to obey Eq. (8).

It is thus the Fjørtoft argument that robustly predicts that particles accumulate at the largest available scale in the system, while energy is lost by the dissipation at

k_{\max} , a process of simultaneous nonequilibrium condensation and evaporation/cooling [48].

The Fjørtoft argument does not specify whether the invariants move via local scale-by-scale interactions, or by a direct transfer from the intermediate to the extremal scales. In the next Sec. IID we consider spectra on which the two invariants move via a local cascade.

D. Kolmogorov-Zakharov flux spectra as formal solutions of the kinetic equation

The landmark result of the theory of weak wave turbulence is the discovery of spectra in which invariants move with constant flux through \mathbf{k} -space via a local scale-by-scale cascade, potentially realising the predictions of the Fjørtoft argument. (However, anticipating the results of Sec. IIF, it turns out that for the Schrödinger-Newton Eqs. (3) and nonlinear Schrödinger Eq. (2) these spectra lead in most cases to cascades with the fluxes in the wrong direction, a contradiction that we resolve in the remainder of this work.) These are the Kolmogorov-Zakharov spectra [1] and are analogous to Kolmogorov's famous $k^{-5/3}$ energy cascade spectrum for 3D classical strongly-nonlinear hydrodynamical turbulence [49]. When they exist, they are steady nonequilibrium solutions of the kinetic equation in which the spectra are scale-invariant, i.e.

$$n_{\mathbf{k}} \propto k^{-x}. \quad (11)$$

Necessary (but not sufficient) conditions for such spectra to exist are that both the dispersion relation and interaction coefficient are themselves both scale-invariant. In our case, all equations of the nonlinear Schrödinger type have a dispersion relation $\omega_{\mathbf{k}} = k^2$. For the interaction coefficient we require a homogeneous function in the sense that

$$W_{\mu\mathbf{k}_3 \mu\mathbf{k}_4}^{\mu\mathbf{k}_1 \mu\mathbf{k}_2} = \mu^\beta W_{\mathbf{k}_3 \mathbf{k}_4}^{\mathbf{k}_1 \mathbf{k}_2}.$$

For the Schrödinger-Helmholtz Eqs. (1) we obtain a scale-invariant interaction coefficient in either the Schrödinger-Newton limit $\ell \ll \ell_*$ (in which case $\beta = -2$) or in the nonlinear Schrödinger limit $\ell \gg \ell_*$ (where $\beta = 0$).

The Kolmogorov-Zakharov spectra are obtained by making a so-called Zakharov-Kraichnan transform in the kinetic equation (8) and using the scaling behaviour of all quantities under the integral [1, 2, 37], or via dimensional analysis [2, 50]. We omit the details and quote the results here.

For systems of $2 \leftrightarrow 2$ wave scattering in d spatial dimensions, the spectrum that corresponds to a *constant flux of particles* and zero flux of energy has index

$$x_{\text{FN}} = d + \frac{2\beta}{3} - \frac{2}{3}. \quad (12a)$$

The spectrum of *constant energy flux* with zero particle flux is

$$x_{\text{FE}} = d + \frac{2\beta}{3}. \quad (12b)$$

⁴ See also Chapter 4 of [2] that makes a modified argument that does not rely on the system being open.

In particular for the Schrödinger-Newton Eqs. (3) we have $\beta = -2$, so

$$x_{\text{FN}} = 1, \quad x_{\text{FE}} = 5/3 \quad \text{for} \quad d = 3, \quad (13a)$$

$$x_{\text{FN}} = 0, \quad x_{\text{FE}} = 2/3 \quad \text{for} \quad d = 2, \quad (13b)$$

while for the nonlinear Schrödinger Eq. (2) $\beta = 0$, so

$$x_{\text{FN}} = 7/3, \quad x_{\text{FE}} = 3 \quad \text{for} \quad d = 3, \quad (13c)$$

$$x_{\text{FN}} = 4/3, \quad x_{\text{FE}} = 2 \quad \text{for} \quad d = 2. \quad (13d)$$

Results (13c) and (13d) are known [1, 2, 37] but the pure-flux Kolmogorov-Zakharov spectra Eqs. (13a) and (13b) for the Schrödinger-Newton equation are new results that we report for the first time here.

E. Equilibrium spectra

The kinetic equation redistributes E and N over the degrees of freedom (wave modes) as it drives the system to thermodynamic equilibrium. At the end of the evolution equilibrium is reached when the invariant $\sigma = (E + \mu N)/T$ is distributed evenly across all wave modes. This is realised by the Rayleigh-Jeans spectrum⁵

$$n_{\mathbf{k}} = \frac{T}{\omega_{\mathbf{k}} + \mu}, \quad (14)$$

where T is the temperature and μ is the chemical potential.

In particular the spectrum is scale invariant, satisfying Eq. (11), when there is equipartition of particles only (the thermodynamic potentials $\mu, T \rightarrow \pm\infty$ such that $T/\mu = n_{\mathbf{k}} = \text{const}$) or of energy only (obtained when $\mu = 0$). We denote the corresponding spectral indices for thermodynamic equipartition of particles and energy, respectively, as

$$x_{\text{TN}} = 0 \quad \text{and} \quad x_{\text{TE}} = 2. \quad (15)$$

F. Directions of the energy and particle fluxes and realisability of the scale-invariant spectra

With the various indices for the stationary Kolmogorov-Zakharov and Rayleigh-Jeans power-law spectra in hand, we now turn to the following simple argument to determine the directions of the particle and energy fluxes $\eta(x)$ and $\epsilon(x)$.

We consider what the flux directions will be when the spectrum is a power-law as in Eq. (11). We expect the

fluxes to respond to a very steep spectrum by spreading the spectrum out. Therefore for x large and positive (spectrum sharply increasing towards low wavenumber) we expect both $\eta, \epsilon > 0$, and for x large and negative (spectrum ramping at high wavenumber) we expect $\eta, \epsilon < 0$. Furthermore, both fluxes will be zero for both thermal equilibrium exponents x_{TN} and x_{TE} . Finally the waveaction flux vanishes for the pure energy flux spectrum with exponent x_{FE} , and the energy flux vanishes for the pure particle flux exponent x_{FN} . By continuity the signs of both fluxes for all x are fully determined by their signs at infinity and the locations of their zero crossings. The fluxes will schematically vary in the manner shown in Fig. 1(a,b) for the Schrödinger-Newton model and Fig. 1(c,d) for the nonlinear Schrödinger model.

First we consider the Schrödinger-Newton equation. In both 3D and 2D at the spectral index corresponding to pure energy flux x_{FE} we find that ϵ is negative. On x_{FN} , the pure particle flux spectrum, we find that η is negative in 3D, whereas in 2D there is a degeneracy with the particle equipartition spectrum $x_{\text{FN}} = x_{\text{TN}}$ and correspondingly $\eta = 0$ there. These findings are in contradiction to the Fjørtoft argument.

For the nonlinear Schrödinger equation in 3D ϵ is positive at x_{FE} and η is negative at x_{FN} . This is in agreement with the Fjørtoft argument. We therefore naively expect that in 3D the Kolmogorov-Zakharov flux cascades are possible. It turns out that the inverse particle Kolmogorov-Zakharov spectrum is realised, with a scale-by-scale transfer of particles to small scales, however the direct energy cascade is nonlocal and the spectrum must be modified to correct a logarithmic divergence in the infrared limit, see refs. [2, 37] for details.

For the 2D nonlinear Schrödinger equation the energy flux and equipartition spectra are degenerate $x_{\text{FE}} = x_{\text{TE}}$, giving $\epsilon = 0$ there, and at the particle flux spectral index x_{FN} we find η is positive.

These results for the Schrödinger-Newton equation and 2D nonlinear Schrödinger equation are in contradiction to the Fjørtoft argument of a forward energy cascade and inverse particle cascade. However the Fjørtoft argument is robust and predicts that if an initial spectrum evolves, it must push most of the energy towards small scales and particles towards large scales. We therefore conclude that the Schrödinger-Newton Eqs. (3), and the nonlinear Schrödinger Eq. (2) in 2D, do not accomplish this via the Kolmogorov-Zakharov spectra that are determined solely by the values of the flux. To resolve this paradox we develop a simplified theory to reduce the integro-differential kinetic equation to a partial differential equation that is analytically tractable.

G. Differential approximation model for wave turbulence

The Kolmogorov-Zakharov solutions of the kinetic equation for the Schrödinger-Newton equation in 3D

⁵ Formally, achieving the Rayleigh-Jeans spectrum depends on there being a small-scale cutoff k_{max} to prevent σ being shared over an infinite number of wave modes, i.e. the trivial solution $n_{\mathbf{k}} = 0$ for every \mathbf{k} .

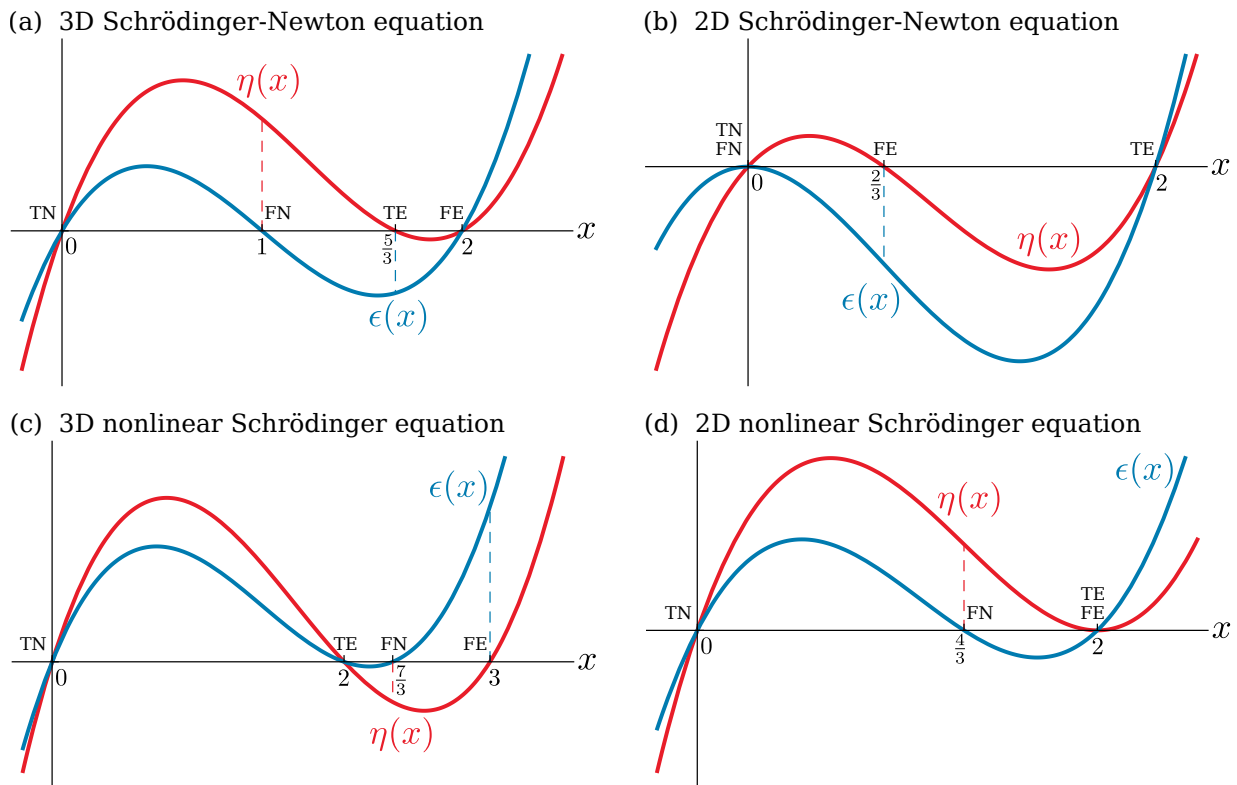


FIG. 1: Particle flux $\eta(x)$ (in red) and energy flux $\epsilon(x)$ (in blue) as a function of spectral index x for the limits of the Schrödinger-Helmholtz model. Upper panels for the Schrödinger-Newton model in (a) $d = 3$, and (b) in $d = 2$. Lower panels for the nonlinear Schrödinger model in (c) $d = 3$, and (d) $d = 2$. Dashed lines indicate the signs of the fluxes when the spectral index takes the values x_{FN} and x_{FE} .

and 2D, and for the nonlinear Schrödinger equation in 2D predict the wrong directions for the fluxes as compared to the Fjørtoft argument. Such solutions cannot be realised for any finite scale separation between forcing and dissipation. From experience with other wavenumber systems we expect that the flux-carrying spectra in these cases are instead close to the zero-flux thermal Rayleigh-Jeans solutions, but with deviations that carry the flux [2, 51, 52]. These deviations are small deep inside the inertial ranges but become large at the ends, making the spectrum decay rapidly to zero near the dissipation scales. Spectra of this sort are termed “warm” cascades [51, 53–55]. A feature of these solutions is that the thermodynamic potentials T and μ will be functions of the flux they have to accommodate⁶, and the scales at which the spectrum decays, i.e.

$$\frac{T}{\mu} = f(\eta, \omega_{\min}) \quad (16)$$

⁶ Note that the temperature T of the warm cascade refers to the energy shared between wave modes, and is not related to the temperature of particle or molecular degrees of freedom of the material at hand (Boson gas or nonlinear optical sample), which plays no role in this analysis.

for the inverse cascades and

$$T = g(\epsilon, \omega_{\max}) \quad (17)$$

for direct cascades [2, 51, 52], where the functional forms of f and g are to be found, and we have converted from wavenumber to frequency using the dispersion relation $\omega = k^2$ (we will continue to refer to “scales” when discussing frequencies as the isotropy of the spectrum allows us to use the dispersion relation to convert between spatial and temporal scales).

To describe warm cascade states we develop a differential approximation model that simplifies the kinetic equation by assuming that interactions are super-local in frequency space ($\omega_k \approx \omega_1 \approx \omega_2 \approx \omega_3$). This allows the collision integral to be reduced to a purely differential operator. Asymptotically-correct stationary solutions of this reduced model can then be found analytically, and these will be qualitatively similar to the solutions for the full kinetic equation [37, 51–56].

The reduction of the general 4-wave kinetic equation to the differential approximation model is done explicitly in Ref. [37]. Here we take a heuristic approach based on the scaling of the kinetic equation and neglect the full calculation of numerical prefactors.

We integrate over angles in \mathbf{k} -space and change variables to frequency. The general form of the differen-

tial approximation model is then an ordinary differential equation in local conservative form

$$\omega^{d/2-1} \frac{\partial n}{\partial t} = \frac{\partial^2 R}{\partial \omega^2}, \quad (18a)$$

where $n = n(\omega)$ is the spectrum expressed as a function of ω , and the quantity

$$R = S\omega^\lambda n^4 \frac{\partial^2}{\partial \omega^2} \left(\frac{1}{n} \right) \quad (18b)$$

is constructed so as to ensure that the Rayleigh-Jeans spectrum is a stationary solution [$\partial_{\omega\omega}(1/n)$ term], the n^4 term derives from the fact that 4-wave interactions are responsible for the spectral evolution, the total n scaling matches the kinetic equation, and S is a constant.

To find λ for the systems considered in the present work we examine how the kinetic Eq. (8) scales with ω . Schematically the kinetic equation is

$$\dot{n} = \int W^2 n^3 \delta(\mathbf{k}) \delta(\omega) (d\mathbf{k})^3 \sim n^3 k^{2\beta+2d-2} \sim n^3 \omega^{\beta+d-1}$$

while the differential approximation evolution equation (18a) scales as

$$\omega^{d/2-1} \dot{n} \sim n^3 \omega^{\lambda-4}.$$

Comparing powers of ω we find that

$$\lambda = \beta + \frac{3d}{2} + 2. \quad (19)$$

H. Fluxes in the differential approximation

Comparing Eq. (18a) with (10a) and (10b) we see that the particle and energy fluxes expressed as a function of ω are, up to a geometrical factor that can be absorbed into S ,

$$\eta = -\frac{\partial R}{\partial \omega} \quad \text{and} \quad \epsilon = -\omega \frac{\partial R}{\partial \omega} + R. \quad (20)$$

respectively.

Putting a power law spectrum $n = \omega^{-x/2}$ into Eqs. (18a), (18b) and (20) allows us to find expressions for the fluxes. The particle flux is

$$\eta = -\frac{x}{2} \left(\frac{x}{2} - 1 \right) \left(\beta + \frac{3d}{2} - \frac{3x}{2} \right) S \omega^{\beta+3d/2-3x/2-1}$$

and vanishes when $x = 0$ or $x = 2$, corresponding to the thermodynamic particle and energy spectral indices of Eqs. (15). The particle flux also vanishes when $x = d + \frac{2\beta}{3}$, corresponding to the energy flux spectral index x_{FE} of Eqs. (13a) to (13d). The energy flux is

$$\epsilon = -\frac{x}{2} \left(\frac{x}{2} - 1 \right) \left(\beta + \frac{3d}{2} - \frac{3x}{2} - 1 \right) S \omega^{\beta+3d/2-3x/2} \quad (21)$$

and is again zero for the Rayleigh-Jeans spectra where $x = 0$ or $x = 2$, and for the constant particle flux/zero energy flux Kolmogorov-Zakharov spectrum with $x = d + \frac{2\beta}{3} - \frac{2}{3}$.

Thus in the differential approximation model we recover the results of Secs. IID and IIE. Furthermore, this model gives a quantitative prediction of $\eta(x)$ and $\epsilon(x)$ for all values of x (to within the limits of the super-local assumption, and the numerical determination of S). For example taking $S = 1$ and $\omega = 1$ we have the cubic functions

$$\eta = -\frac{x}{2} \left(\frac{x}{2} - 1 \right) \left(\beta + \frac{3d}{2} - \frac{3x}{2} \right), \quad (22a)$$

$$\epsilon = -\frac{x}{2} \left(\frac{x}{2} - 1 \right) \left(\beta + \frac{3d}{2} - \frac{3x}{2} - 1 \right), \quad (22b)$$

that are drawn in Fig. 1, with $\beta = -2$ for the Schrödinger-Newton Eqs. (3) and $\beta = 0$ for the nonlinear Schrödinger Eq. (2).

III. TURBULENT SPECTRA IN THE SCHRÖDINGER-HELMHOLTZ MODEL

A. Reconciling with the Fjørtoft argument

Having established the cases in which the Kolmogorov-Zakharov spectra give either the wrong direction of the fluxes or zero fluxes for the Schrödinger-Newton and the nonlinear Schrödinger models, we now seek the spectra that give the correct fluxes. To agree with the Fjørtoft argument we require a spectrum for the direct inertial range that carries the constant positive energy flux ϵ from the forcing scale ω_f up to the dissipation scale ω_{max} , but carries no particles. Setting $\eta = \partial_\omega R = 0$ in eqs. (20) we obtain the ordinary differential equation

$$\epsilon = R = \text{const} > 0 \quad (23)$$

in the direct inertial range.

Likewise in the inverse inertial range we require a spectrum that carries the constant negative particle flux η from ω_f to dissipate at ω_{min} , but carries zero energy. Setting $\epsilon = 0$ in Eq. (20) we obtain $\partial_\omega R = R/\omega$ and so

$$\eta = -\frac{R}{\omega} = \text{const} < 0 \quad (24)$$

in the inverse inertial range.

We now proceed in turn through the 3D and 2D Schrödinger-Newton equation, followed by the 2D nonlinear Schrödinger equation, and use Eqs. (23), and (24) to resolve the predictions from Sec. IIF that are in conflict with the Fjørtoft argument.

(A full qualitative classification of the single-flux stationary spectra in the differential approximation model for 4-wave turbulence is presented in Ref. [57], based on the phase space analysis of an auxiliary dynamical system. Those general results are relevant to the systems

under consideration in this paper, however here we will concentrate on the particular functional form of the flux-carrying spectra in the inertial range, and establish the relationships (16), (17) between the thermodynamic potentials and the fluxes, in the spirit of Refs. [2, 51, 52].)

B. Spectra in the 3D Schrödinger-Newton model

In Sec. IIF we found that in the 3D Schrödinger-Newton Eqs. (3) both the particle and the energy cascade had the wrong sign on their respective Kolmogorov-Zakharov spectra. We specialise Eq. (19) to this model by setting $\beta = -2$ and $d = 3$ and, following Ref. [2], we use the ordinary differential Eqs. (23) and (24) to seek warm cascade solutions that carry the fluxes in the directions predicted by Fjørtoft's argument.

1. Warm inverse particle cascade in the 3D Schrödinger-Newton model

The warm cascade is an equilibrium Rayleigh-Jeans spectrum with a small deviation. Thus we propose the spectrum

$$n = \frac{T}{\omega + \mu + \theta(\omega)} \quad (25)$$

and assume that the disturbance $\theta(\omega)$ is small deep in the inverse inertial range i.e. $\omega_{\min} \ll \omega \ll \omega_f$. We substitute this into Eq. (18b) and impose the constant-flux condition (24) for the inverse cascade. Linearising with respect to the small disturbance, we obtain the equation

$$\theta''(\omega) = -\frac{\eta}{ST^3} \frac{(\omega + \mu)^4}{\omega^{7/2}}.$$

Integrating twice, and noting that $|\eta|$ is negative, yields the following expression for the deviation away from the thermal spectrum that is valid deep in the inertial range

$$\theta(\omega) = \frac{|\eta|}{ST^3} \left(\frac{4\omega^{5/2}}{15} + \frac{16\mu\omega^{3/2}}{3} - 24\mu^2\omega^{1/2} + \frac{16\mu^3}{3\omega^{1/2}} + \frac{4\mu^4}{15\omega^{3/2}} \right), \quad (26)$$

where we have absorbed the two integration constants by renormalising T and μ .

We can use (26) to obtain a relation between the flux and thermodynamic parameters of the form (16) via the following ‘‘approximate matching’’ argument. We need the warm cascade spectrum to terminate at the dissipation scale ω_{\min} . Therefore near the dissipation scale we expect $\theta(\omega)$ to become significant, compared to the other terms in the denominator of (25), i.e. we expect $\theta(\omega) \sim \omega + \mu$ near ω_{\min} . We put these terms into balance

at ω_{\min} and assume the ordering⁷ $\omega_{\min} \ll \mu$. Taking the leading term from Eq. (26), we obtain the flux scaling

$$\left(\frac{T}{\mu}\right)^3 \sim \frac{4}{15S} |\eta| \omega_{\min}^{3/2}. \quad (27)$$

Of course this matching procedure is not strictly rigorous as Eq. (26) was derived for small θ and we are extending it to where θ is large. Nevertheless, we expect that the scaling relation (27) will give the correct functional relationship between the thermodynamic parameters and the flux and dissipation scale. (Results derived in a similar spirit in other systems give predictions that agree well with direct numerical simulations, see e.g. Ref. [51].)

Now we examine the structure of the inverse cascade near the dissipation scale. Assuming that the spectrum around $(\omega - \omega_{\min}) \ll \omega_{\min}$ is analytic, the condition $n(\omega_{\min}) = 0$ suggests that the spectrum terminates in a compact front whose leading-order behaviour is of the form $n = A(\omega - \omega_{\min})^\sigma$. Again we substitute this ansatz into Eq. (18b), and demand that the flux is carried all the way to the dissipation scale, i.e. we impose the condition (24). Requiring that the flux is frequency-independent fixes A and σ , and we obtain the compact front solution at the dissipation scale

$$n = \left(\frac{9|\eta|}{10S\omega_{\min}^{7/2}} \right)^{1/3} (\omega - \omega_{\min})^{2/3}. \quad (28)$$

We shall find below that the compact front solution is nearly identical near each dissipation range in each model and dimensionality that we examine. This is because the $\sim n^3$ scaling of the spectrum in Eq. (18b), and the need for the compact front to vanish at the respective dissipation scale ω_* fixes $\sigma = 2/3$. The only difference will be the flux and the power of the respective ω_* in the coefficient, and the sign difference in the power law.

We note that Eq. (26) suggests that $\theta(\omega)$ could again become large at high frequency. Arguing as above, this permits the spectrum to terminate at a compact front at frequency $\omega_+ > \omega_{\min}$. One could argue likewise for the warm direct energy cascade spectrum, see Eq. (29) below. Indeed all the warm cascade spectra discussed in this paper contain the possibility that they might be bounded by two compact fronts. We discuss this matter in the Appendix.

Using the differential approximation we have shown how the inverse cascade of particles in the 3D Schrödinger-Newton Eqs. (3) is carried by a warm cascade that closely follows a Rayleigh-Jeans spectrum in the inertial range, with a strong deviation near the dissipation scale that gave us an approximate scaling relation

⁷ If instead we set $\omega_{\min} \sim \mu$ or $\omega_{\min} \gg \mu$ then $\theta(\omega)$ would not become small for any $\omega \geq \omega_{\min}$, contradicting the assumption under which we derived eq. (26).

between the thermodynamic parameters and the cascade parameters. We also investigated the structure of the spectrum at the dissipation scale and found it to be a compact front with a $\frac{2}{3}$ -power law that vanishes at ω_{\min} .

In the rest of this work we will use the same procedures, with the model and dimensionality under consideration giving us the appropriate ω -scaling in the differential approximation, to identify similar features of the cascades. First, we turn to the direct cascade of energy in the 3D Schrödinger-Newton Eqs. (3).

2. Warm direct energy cascade in the 3D Schrödinger-Newton model

To find a direct cascade of energy for the 3D Schrödinger-Newton equation we again use the warm cascade ansatz (25) and this time impose the constant energy flux condition (23). We go through the same approximate matching procedure as in Sec. III B 1: we find $\theta(\omega)$ under the assumption that it is small,

$$\theta(\omega) = \frac{\epsilon}{ST^3} \left(\frac{4\omega^{3/2}}{3} - 16\mu\omega^{1/2} + \frac{8\mu^2}{\omega^{1/2}} + \frac{16\mu^3}{15\omega^{3/2}} + \frac{4\mu^4}{35\omega^{5/2}} \right), \quad (29)$$

where again we have absorbed the two integration constants into T and μ . Extending (29) towards ω_{\max} where we require it to balance the other terms in the denominator of (25), and assuming⁸ $\mu \ll \omega_{\max}$ gives a scaling relation of the type (17)

$$T^3 \sim \frac{4}{3S} \epsilon \omega_{\max}^{1/2}. \quad (30)$$

In the immediate vicinity of ω_{\max} we again expect a compact front. Substituting $n = A(\omega_{\max} - \omega)^\sigma$ into (23) gives the leading-order structure

$$n = \left[\frac{9\epsilon(\omega_{\max} - \omega)^2}{10S\omega_{\max}^{9/2}} \right]^{1/3}. \quad (31)$$

Again we note that Eq. (29) suggests that θ can be made large at some low frequency that would lead to a second compact-front cutoff at $\omega_- < \omega_{\max}$. All the warm cascade spectra we discuss here have the potential to be terminated at two compact fronts. This is discussed in the Appendix.

3. Warm dual cascade in the 3D Schrödinger-Newton model

In summary, the results of Secs. III B 1 and III B 2 predict that for the 3D Schrödinger-Newton model in the

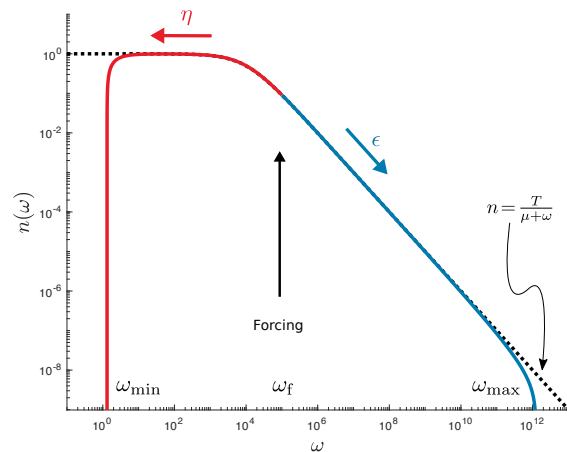


FIG. 2: Dual warm cascade in the 3D Schrödinger-Newton equations. The inverse particle cascade, with negative particle flux η , is shown in red. In blue is the direct energy cascade with positive flux ϵ . The black dashed line is the thermodynamic equipartition spectrum (14). (See main text for parameters.)

forced-dissipative setup, the movement of particles to large scales and energy to small scales is realised by a dual warm cascade spectrum. This spectrum starts close to the Rayleigh-Jeans distribution (14) near the forcing scale ω_f and then deviates strongly away, until it vanishes at compact $2/3$ power-law fronts at the dissipation scales ω_{\min} and ω_{\max} . We show the dual warm cascade in Fig. 2, which was obtained by numerically integrating Eq. (23) forwards and Eq. (24) backwards from the initial condition that the spectrum and its derivative matched the Rayleigh-Jeans spectrum (14) at $\omega_f = 10^5$, with $T = \mu = 10^4$. The warm cascades carry a particle flux $\eta = -3.75$ to large scales and energy flux $\epsilon = \omega_f^2 |\eta|$ to small scales, and the geometric constant $S = 1$.

The dual warm cascade for the 2D Schrödinger-Newton and 2D nonlinear Schrödinger models can be obtained in a similar fashion. They are qualitatively similar to Fig. 2 so we omit displaying them.

C. Spectra in the 2D Schrödinger-Newton model

Now we turn to the 2D Schrödinger-Newton Eqs. (3), setting $\beta = -2$ and $d = 2$ in Eq. (19). In Sec. II F we found that the particle equipartition and cascade spectra coincided, making the particle flux zero, and that the energy flux had the wrong sign.

1. Log-corrected inverse particle cascade in the 2D Schrödinger-Newton model

The degeneracy between the particle Rayleigh-Jeans and Kolmogorov-Zakharov spectra $n \sim \omega^0$ can be

⁸ For $\omega_{\max} \sim \mu$ or $\omega_{\max} \gg \mu$ there is no range of $\omega \leq \omega_{\max}$ for which $\theta(\omega)$ is small.

lifted by making a logarithmic correction to this spectrum. Substituting the trial solution $n = B \ln^z(\omega/\omega_{\min})$ into Eq.(18b) and enforcing constant negative particle flux (24) that is independent of ω gives

$$n = \left[\frac{3|\eta|}{S} \ln\left(\frac{\omega}{\omega_{\min}}\right) \right]^{1/3} \quad (32)$$

to leading order deep in the inverse inertial range.

To find a relation between the thermodynamic parameters and the cascade parameters we carry out the approximate matching procedure described in Sec. III B 1 at low frequency $\omega \sim \omega_{\min} \ll \mu$, obtaining

$$\left(\frac{T}{\mu}\right)^3 \sim \frac{|\eta|}{S} \ln \omega_{\min}. \quad (33)$$

As $\omega \rightarrow \omega_{\min}$ the spectrum in Eq. (32) becomes zero, as we would expect given ω_{\min} is a dissipation scale. However we note that this is only a qualitative statement as subleading terms will start to dominate in this limit, meaning that Eq.(32) is no longer the correct stationary spectrum there. To obtain the correct leading-order structure near ω_{\min} we look for a compact front solution and find once again a $2/3$ power law,

$$n = \left[\frac{9|\eta|}{10S} \left(\frac{\omega - \omega_{\min}}{\omega_{\min}}\right)^2 \right]^{1/3}. \quad (34)$$

2. Warm direct energy cascade in the 2D Schrödinger-Newton model

To find a forward energy cascade for the 2D Schrödinger-Newton model we again look for a warm cascade, substituting Eq. (25) into (18b) and seeking a constant energy flux (23). Solving for the perturbation and matching the deviation to the other terms in the denominator in (25) at $\omega \sim \omega_{\max} \gg \mu$ gives the scaling relation

$$T^3 \sim \frac{\epsilon \omega_{\max}^2}{6S}.$$

The compact front near ω_{\max} has leading-order form

$$n = \left[\frac{9\epsilon(\omega_{\max} - \omega)^2}{10S\omega_{\max}^3} \right]^{1/3}. \quad (35)$$

D. Spectra in the 2D nonlinear Schrödinger model

In Sec.IIF we found that the Kolmogorov-Zakharov particle flux spectrum for the nonlinear Schrödinger model was positive rather than negative, and that the Kolmogorov-Zakharov energy flux spectrum coincides with the Rayleigh-Jeans energy equipartition spectrum. We specialise to the 2D nonlinear Schrödinger Eq. (2) by setting $\beta = 0$ and $d = 2$ in Eq. (19) and take these issues in turn. (These results recapitulate and extend the discussion in Chapter 15 of Ref. [2].)

1. Warm inverse particle cascade in the 2D nonlinear Schrödinger model

The approximate matching procedure described above gives the scaling relation

$$\left(\frac{T}{\mu}\right)^3 \sim \frac{|\eta|}{6S\omega_{\min}^2}$$

for the inverse cascade. The compact front solution at the dissipation scale has the structure

$$n = \left[\frac{9|\eta|(\omega - \omega_{\min})^2}{10S\omega_{\min}^4} \right]^{1/3}. \quad (36)$$

2. Log-corrected direct energy cascade in the 2D nonlinear Schrödinger model

The degeneracy of $n \propto \omega^{-1}$ corresponding to both the Kolmogorov-Zakharov energy flux spectrum and the Rayleigh-Jeans energy equipartition spectrum can be again lifted by making a logarithmic correction. Substituting the spectrum $n = (B/\omega) \ln^z(\omega_{\max}/\omega)$ into Eq. (18b) and imposing Eq. (23) we obtain

$$n = \frac{1}{\omega} \left[\frac{3\epsilon \ln(\omega_{\max}/\omega)}{S} \right]^{1/3}. \quad (37)$$

Comparing Eq. (37) to the energy equipartition spectrum $n = T/\omega$ we have a relation of the kind in Eq.(17), namely

$$T^3 \sim \frac{3\epsilon}{S} \ln \omega_{\max}. \quad (38)$$

We obtain the same scaling [apart from the factor of 3 on the right-hand side of Eq. (38)] if we assume a warm cascade and carry out the approximate matching procedure as described in Sec. III B 1. This is natural as the log-corrected solution (37) is of a prescribed form whereas in the warm cascade argument the perturbation θ is not constrained from the outset, so the two solutions are two different perturbations from the thermal spectrum. However by continuity they should give the same scaling of thermal with cascade parameters, differing only by an $\mathcal{O}(1)$ constant.

As in Sec. III C 1 the log-corrected spectrum (37) becomes zero at the dissipation scale. However the structure will not be correct here as sub-leading terms would start to become significant. The correct leading-order structure for the front is again the $2/3$ power-law

$$n = \left[\frac{9\epsilon(\omega_{\max} - \omega)^2}{10S\omega_{\max}^5} \right]^{1/3}.$$

E. Crossover from warm to Kolmogorov-Zakharov cascade in the 2D Schrödinger-Helmholtz model

As mentioned in Sec. IIF the dual cascade in the 3D nonlinear Schrödinger limit of (1) is achieved by a scale-invariant Kolmogorov-Zakharov spectrum, rather than the warm cascade discussed in Sec. IIIB for the 3D Schrödinger-Newton limit. Both these two regimes may be accessed if the removal of waveaction from the weakly-nonlinear wave content of the system (through dissipation or absorption into the condensate) is situated at larger scales than the cosmological constant which controls the crossover between the two limits of Eqs. (1), i.e. if $\omega_{\min} \ll \Lambda$. We sketch this schematically in Fig. 3(a) when $\omega_f \gg \Lambda$, so the crossover from the Kolmogorov-Zakharov to the warm cascade happens in the inverse inertial range, and in Fig. 3(b) when $\omega_f \ll \Lambda$ and the crossover happens in the direct inertial range.

Note that Fig. 3 is a sketch and not produced directly by using the stationary differential approximation model (20). This is because in the crossover regime $\omega \approx \Lambda$ the interaction coefficient (6d) cannot be put into scale-invariant form. Accurate realisations of Fig. 3 must await direct numerical simulation of Eqs. (1) in future work.

The crossover from a scale-invariant cascade dominated by flux to an equipartition-like spectrum at small scales is common in turbulence, when a flux-dominated spectrum runs into a scale where the flux stagnates and thermalises. The stagnation is due to a mismatch of flux rate between the scale-invariant spectrum and the small-scale processes, whether that be (hyper-)dissipation in hydrodynamic turbulence [53, 58], or a different physical regime such as the crossover from hydrodynamic to Kelvin wave turbulence in superfluids [59]. Our case here, the crossover from the nonlinear Schrödinger to the Schrödinger-Newton regime, is more like the latter but again the details await further work.

IV. CONCLUSION AND OUTLOOK

In this work we have developed the theory of weak wave turbulence in the Schrödinger-Helmholtz Eqs. (1), which contain as limits both the nonlinear Schrödinger and Schrödinger-Newton Eqs. (2) and Eqs. (3). We obtained the kinetic equation for the Schrödinger-Helmholtz model in the case of 4-wave turbulence, that is of random fluctuations of the field with no condensate present, and we used the Fjørtoft argument to predict the dual cascade of particles upscale and energy downscale in this model.

Using the differential approximation to the full kinetic equation, we have characterised the statistically steady states of its Schrödinger-Newton and nonlinear Schrödinger limits in the case of a forced-dissipated system. We found that the dual cascade is achieved via a warm spectrum for the Schrödinger-Newton limit in 2D and 3D, and for the nonlinear Schrödinger limit in 2D.

For the 3D nonlinear Schrödinger limit the Kolmogorov-Zakharov spectra are responsible for the cascades, and we have schematically illustrated the crossover between the warm and Kolmogorov-Zakharov cascades when both limits of the full Schrödinger-Helmholtz model are accessible.

Finally we found scaling relationships between the thermodynamic parameters and the fluxes and dissipation scales of the type (16) and (17) for these cascades. We have thus characterised the processes by which particles are condensed at the largest scales, and energy sent to small scales, in both limits of the Schrödinger-Helmholtz model. The results for the nonlinear Schrödinger model have already appeared in the literature before, but the results for the Schrödinger-Newton model are new and are relevant to the problem of cosmological structure formation in a fuzzy dark matter universe, and to optical systems where the thermo-optic effect is significant.

Focusing on the astrophysical application, our results suggest that a warm dual cascade described by weak wave turbulence is the first process that starts to accumulate a condensate of dark matter particles at large scales in the early universe. We speculate that following this initial phase of condensation the subsequent evolution will follow the same lines as has already been broadly documented in the literature, namely that gravitational collapse of the condensate will ensue, via 2D filamentation followed by collapse into a collection of virialised 3D spheroidal haloes [23].

We also speculate that wave turbulence may have much to say regarding certain other details that have already been noted. For example, the structure of haloes has been reported as a solitonic core that is free of turbulence surrounded by a turbulent envelope [22]. The exclusion of turbulence from the core is reminiscent of the externally-trapped defocusing nonlinear Schrödinger Eq. (2), where wave turbulence combined with wavepacket (Wentzel-Kramers-Brillouin) analysis predicts the refraction of Bogoliubov sound waves towards the edges of a condensate, where transition from the three-wave Bogoliubov wave turbulence to four-wave processes could occur [48]. On the other hand the virialisation of haloes suggests a condition of critical balance where the linear propagation and nonlinear interaction timescales of waves are equal scale by scale. In that case the weak wave turbulence described here is not applicable and new spectral relations must be found based on the critical balance hypothesis [2, 60].

After the formation of haloes the next step of the evolution will be their mutual interaction. In the 1D nonlinear Schrödinger equation, with six-wave interactions taken into account to break the integrability of the system, it has been observed in simulations and experiments that a random field creates a condensate via the dual cascade, which then collapses into solitons. These solitons then interact via the exchange of waves and finally merge into one giant soliton that dominates the dynam-

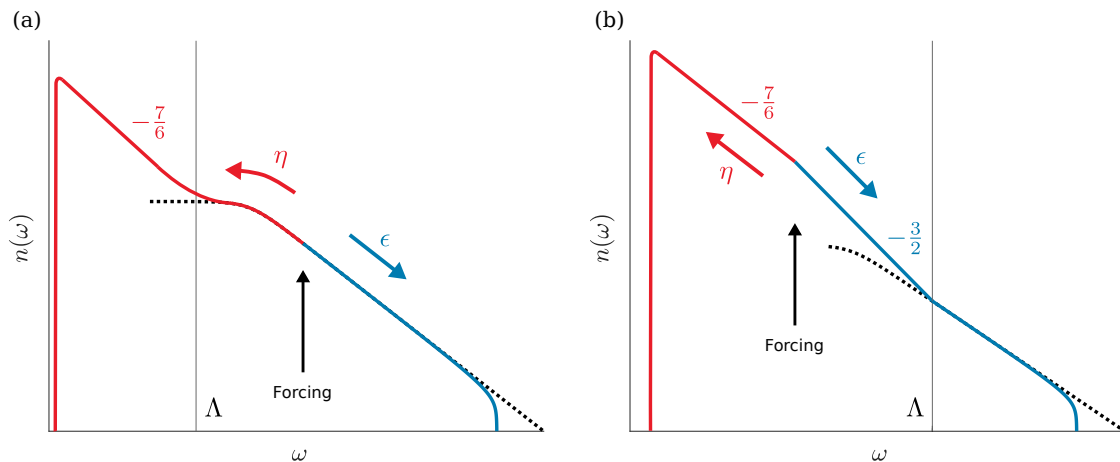


FIG. 3: Sketch of the crossover from a warm cascade [which follows closely the thermodynamic spectrum (14) shown in black dashes] to a scale-free cascade, the latter with the Kolmogorov-Zakharov spectral indices shown. The crossover happens around $\omega \approx \Lambda$, with the warm cascade in $\omega \gg \Lambda$ and the Kolmogorov-Zakharov cascade in $\omega \ll \Lambda$. Depending on placement of the forcing scale the crossover happens (a) in the inverse cascade (shown in red) or (b) in the direct cascade (shown in blue).

ics [30, 31]. It seems plausible that the same phenomenology might carry over to the Schrödinger-Helmholtz equation, and into higher spatial dimensions. In cosmological simulations of binary and multiple halo collisions, scattering events, inelastic collisions, and mergers are all observed [22, 61–63]. Following such events, subsequent virialisation of the products involves ejection of some of the mass of the haloes [64, 65]. A detailed study of these processes should consider both the weakly nonlinear wave component and the strongly nonlinear haloes, and how the two components interact. Numerical studies could obtain effective collision kernels for those interactions in order to develop a kinetic equation for the “gas” of haloes that results from the collapse of a condensate. We note that work has been done in this spirit in Ref. [63] but without detailed consideration of the wave component. In our opinion it is crucial to incorporate wave turbulence into the study of the Schrödinger-Helmholtz model to uncover the full richness of the behaviour that this system manifests.

Appendix

In Sec. III B we noted that Eqs. (26) and (29) permitted the deviation away from the Rayleigh-Jeans spectrum $\theta(\omega)$ to become large at both low and high frequencies for both the inverse and direct cascades. This led to the intriguing possibility that we could have a warm inverse cascade spectrum, that carries only particles, arising from the cutoff at ω_+ , becoming large at intermediate ω and terminating at the cutoff at ω_{\max} . Similarly one could imagine that the warm direct cascade of energy might exist between ω_- and ω_{\max} , terminating at compact fronts at those frequencies. For both of these to be realised the combined spectrum would have two max-

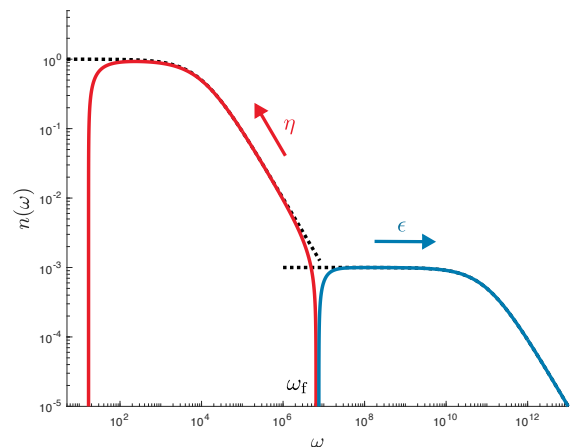


FIG. 4: Double-peaked spectra representing a solution of the differential approximation model where particles are swept upscale (red curve) and energy downscale (blue curve) from forcing at ω_f at a zero value for the spectrum. Black dashed lines represent the two different thermodynamic spectra that match the middle of the two peaks of the spectrum. For parameters see main text.

ima. The frequency where the two cascades met would then be the forcing scale, i.e. $\omega_f = \omega_+ = \omega_-$, and the forcing would be such that all the particles were swept upscale and the energy downscale with the spectrum at ω_f vanishing. This scenario is illustrated in Fig. 4.

(To obtain the direct cascade, shown in blue in Fig. 4, we have integrated (23) forwards to ω_{\max} and backwards to ω_- from a spectrum and its derivative matching Eq. (14) at $\omega = 10^{12}$ with $T = 10^8$ and $\mu = 10^{11}$. Likewise to obtain the inverse cascade shown in red, we integrated (24) backwards to ω_{\min} and forwards to ω_+

from a spectrum and its derivative matching Eq. (14) at $\omega = 10^5$ with $T = \mu = 10^4$. The fluxes were $\eta = -150$ and $\epsilon = \omega_f^2 ||\eta|$ with $\omega_f \approx \omega_- \approx \omega_+ = 6.44 \times 10^6$. In Fig. 4 we have chosen parameters to slightly separate ω_- and ω_+ for clarity.)

We argue here that this scenario, although technically possible within the differential approximation, is implausible for more realistic models like the wave kinetic equation (8) or the original dynamical equation itself [the Schrödinger-Helmholtz system (1) or its limits]. Note that this possibility is common to all the warm cascade spectra we discuss here. Following on from Sec. III B we take the concrete example of the Schrödinger-Newton model in 3D, but similar arguments can be made for either the Schrödinger-Newton model or nonlinear Schrödinger model in 2D. The argument proceeds by seeking compatibility with wide inertial ranges, $\omega_{\min} \ll \omega_+$ for the inverse cascade and $\omega_- \ll \max$ for the direct cascade.

Firstly considering the inverse particle cascade, Eq. (26) and the requirement that there exists a range of $\omega > \omega_{\min}$ for which $\theta(\omega)$ is small, gives the ordering $\omega_{\min} \ll \mu$. This ordering gave the relation (27) between flux and thermodynamic parameters. Now, a cutoff at ω_+ implies that in that vicinity the deviation must become comparable to the other terms in the denominator of the warm spectrum (25). We set $\theta(\omega_+) \sim \mu + \omega_+$ here. If we then let either $\omega_+ \sim \mu$ or $\omega_+ \ll \mu$ and substitute (27) then we obtain $\omega_+ \sim \omega_{\min}$, which is not compatible with a wide inertial range. A scale separation between forcing and dissipation is only possible if we have the ordering $\omega_{\min} \ll \mu \ll \omega_+$ for the inverse cascade.

Next we consider the direct energy cascade. Eq. (29) for the deviation, and the requirement that it must be small for some $\omega < \omega_{\max}$ gives the ordering $\mu \ll \omega_{\max}$. From this we obtained the relation (30). If we have a low-frequency cutoff at ω_- then near there it must match the other terms in the denominator of (25). We set $\theta(\omega_-) \sim \mu + \omega_-$ and consider $\omega_- \sim \mu$ and $\omega_- \gg \mu$. Substituting (30) gives $\omega_- \sim \omega_{\max}$ for these two cases, which is not compatible with a wide inertial range. Therefore for the direct cascade we must have $\omega_- \ll \mu \ll \omega_{\max}$.

Thus if we seek a double-peaked “flux-sweeping” spectrum with the inverse and direct warm cascades joining at ω_f and the spectrum being zero there, then the cascades

could not share the same thermodynamic parameters, as μ must lie deep within the inertial ranges of both cascades. Indeed, to realise such a spectrum in Fig. 4 we have had to choose very different sets of thermodynamic parameters for each inertial range. This is technically possible within the differential approximation, as each steady cascade is described by a second order ordinary differential Eq. (23) or Eq. (24), which only requires for its solution the value of the spectrum and its derivative at the forcing scale.

However when considering a fuller model one must consider a more realistic forcing protocol, for example in simulations setting the spectrum to be drawn from a particular distribution at a certain level in a narrow range around ω_f at each timestep. This sets the amplitude and derivative of the spectrum at the forcing scale at the same prescribed value for both cascades, corresponding to prescription of the thermodynamic parameters T and μ that both cascades share. It is therefore hard to imagine a scenario of forcing which could realise the double-peaked spectrum in a more realistic model like Eqs. (1) or Eq. (8). For example the 4-wave collision integral in Eq. (8) has the effect of smoothing out irregularities in the spectrum, and so we expect that any stationary solution will be at least continuous and differentiable. In this respect, this discussion stands as a cautionary example that the differential approximation includes exotic solutions like the double-peaked spectrum of Fig. 4, that a more physically relevant model would not permit.

Acknowledgments

SN and JS thank Marc Brachet for useful discussions regarding the Jeans swindle and its resolution. SN is supported by the Chaire DExcellence IDEX (Initiative of Excellence) awarded by Université de la Côte d’Azur, France, the EU Horizon 2020 research and innovation programme under the grant agreements No 823937 in the framework of Marie Skłodowska-Curie HALT project and No 820392 in the FET Flagships PhoQuS project and the Simons Foundation Collaboration grant ‘Wave Turbulence’ (Award ID 651471). JS is supported by the UK EPSRC through Grant No EP/I01358X/1.

-
- [1] Vladimir E. Zakharov, Victor S. L’vov, and Gregory Falkovich. *Kolmogorov spectra of turbulence I: Wave turbulence*. Springer Series in Nonlinear Dynamics. Springer, 1992.
 - [2] Sergey Nazarenko. *Wave turbulence*, volume 825 of *Lecture Notes in Physics*. Springer, 2011.
 - [3] Lev Pitaevskii and Sandro Stringari. *Bose-Einstein Condensation and Superfluidity*, volume 164 of *International series of monographs on physics*. Oxford University Press, 2016.
 - [4] E. P. Gross. Structure of a quantized vortex in boson systems. *Il Nuovo Cimento*, 20(3):454–477, 1961.
 - [5] Lev P. Pitaevskii. Vortex lines in an imperfect Bose gas. *Sov. Phys. JETP*, 13(2):451–454, 1961.
 - [6] A. C. Newell and J. V. Moloney. *Nonlinear Optics*. ATIMS Series. Addison-Wesley, Redwood City, CA, 1992.
 - [7] G. B. Whitham. *Linear and Nonlinear Waves*, volume 42 of *Pure and Applied Mathematics: A Wiley-Interscience Series of Texts, Monographs and Tracts*. John Wiley &

- Sons, New York, 1999.
- [8] Wayne Hu, Rennan Barkana, and Andrei Gruzinov. Fuzzy cold dark matter: The wave properties of ultraviolet particles. *Phys. Rev. Lett.*, 85(6):1158–1161, 2000.
- [9] Abril Suárez and Tonatiuh Robles, Victor H. and Matos. A review on the scalar field/Bose-Einstein condensate dark matter model. In Claudia Moreno González, José Edgar Madriz Aguilar, and Luz Marina Reyes Barrera, editors, *Accelerated Cosmic Expansion*, pages 107–142, Cham, 2014. Springer International Publishing.
- [10] Pierre-Henri Chavanis. Self-gravitating Bose-Einstein Condensates. In Xavier Calmet, editor, *Quantum Aspects of Black Holes*, chapter 6, pages 151–194. Springer International Publishing, Cham, 2015.
- [11] Lam Hui, Jeremiah P. Ostriker, Scott Tremaine, and Edward Witten. Ultralight scalars as cosmological dark matter. *Phys. Rev. D*, 95(4):043541, 2017.
- [12] M. R. Baldeschi, G. B. Gelmini, and R. Ruffini. On massive fermions and bosons in galactic halos. *Phys. Lett. B*, 122(3-4):221–224, 1983.
- [13] Jae-weon Lee and In-gyu Koh. Galactic halos as boson stars. *Phys. Rev. D*, 53(4):2236–2239, 1996.
- [14] P. J. E. Peebles. Fluid dark matter. *Astrophys. J. Lett.*, 534(2):L127–L129, 2000.
- [15] J. M. Overduin and P. S. Wesson. Dark matter and background light. *Phys. Rep.*, 402:267–406, 2004.
- [16] P. J. E. Peebles and Bharat Ratra. The cosmological constant and dark energy. *Rev. Mod. Phys.*, 75(2):559–606, 2003.
- [17] Volker Springel, Simon D. M. White, Adrian Jenkins, Carlos S. Frenk, Naoki Yoshida, Liang Gao, Julio Navarro, Robert Thacker, Darren Croton, John Helly, et al. Simulations of the formation, evolution and clustering of galaxies and quasars. *Nature*, 435(7042):629–636, 2005.
- [18] D. H. Weinberg, J. S. Bullock, F. Governato, R. Kuzio de Naray, and Peter A. H. G. Cold dark matter: Controversies on small scales. *Proc. Natl. Acad. Sci. U. S. A.*, 112(40):12249–12255, 2015.
- [19] James S. Bullock and Michael Boylan-Kolchin. Small-scale challenges to the Λ CDM paradigm. *Annu. Rev. Astron. Astrophys.*, 55:343–387, 2017.
- [20] Hsi-Yu Schive, Tzihong Chiueh, and Tom Broadhurst. Cosmic structure as the quantum interference of a coherent dark wave. *Nature Physics*, 10(7):496–499, 2014.
- [21] Monica Colpi, Stuart L. Shapiro, and Ira Wasserman. Boson stars: Gravitational equilibria of self-interacting scalar fields. *Phys. Rev. Lett.*, 57(20):2485–2488, 1986.
- [22] Philip Mocz, Mark Vogelsberger, Victor H. Robles, Jesús Zavala, Michael Boylan-Kolchin, Anastasia Fialkov, and Lars Hernquist. Galaxy formation with BECDM—I. Turbulence and relaxation of idealized haloes. *Monthly Notices of the Royal Astronomical Society*, 471(4):4559–4570, 2017.
- [23] Philip Mocz, Anastasia Fialkov, Mark Vogelsberger, Fernando Becerra, Mustafa A. Amin, Sownak Bose, Michael Boylan-Kolchin, Pierre-Henri Chavanis, Lars Hernquist, Lachlan Lancaster, et al. First star-forming structures in fuzzy cosmic filaments. *Phys. Rev. Lett.*, 123(14):141301, 2019.
- [24] Philip Mocz, Anastasia Fialkov, Mark Vogelsberger, Fernando Becerra, Xuejian Shen, Victor H. Robles, Mustafa A. Amin, Jesús Zavala, Michael Boylan-Kolchin, Sownak Bose, et al. Galaxy formation with BECDM—II. Cosmic filaments and first galaxies. *arXiv preprint arXiv:1911.05746*, 2019.
- [25] M. D. Iturbe Castillo, J. J. Sánchez-Mondragón, and S. Stepanov. Formation of steady-state cylindrical thermal lenses in dark stripes. *Opt. Lett.*, 21(20):1622–1624, 1996.
- [26] Carmel Rotschild, Oren Cohen, Ofer Manela, Mordechai Segev, and Tal Carmon. Solitons in nonlinear media with an infinite range of nonlocality: First observation of coherent elliptic solitons and of vortex-ring solitons. *Phys. Rev. Lett.*, 95(21):213904, 2005.
- [27] Thomas Roger, Calum Maitland, Kali Wilson, Niclas Westerberg, David Vocke, Ewan M. Wright, and Daniele Faccio. Optical analogues of the Newton-Schrödinger equation and boson star evolution. *Nat. Commun.*, 7:13492, 2016.
- [28] Rivka Bekenstein, Ran Schley, Maor Mutzafi, Carmel Rotschild, and Mordechai Segev. Optical simulations of gravitational effects in the Newton-Schrödinger system. *Nat. Phys.*, 11:872–878, 2015.
- [29] Marco Peccianti, Claudio Conti, and Gaetano Assanto. Optical modulational instability in a nonlocal medium. *Phys. Rev. E*, 68(2):025602, 2003.
- [30] Umberto Bortolozzo, Jason Laurie, Sergey Nazarenko, and Stefania Residori. Optical wave turbulence and the condensation of light. *J. Opt. Soc. Am. B*, 26(12):2280–2284, 2009.
- [31] Jason Laurie, Umberto Bortolozzo, Sergey Nazarenko, and Stefania Residori. One-dimensional optical wave turbulence: Experiment and theory. *Phys. Rep.*, 514(4):121–175, 2012.
- [32] Michael K.-H. Kiessling. The “Jeans swindle”: a true story — mathematically speaking. *Adv. Appl. Math.*, 31(1):132–149, 2003.
- [33] James Binney and Scott Tremaine. *Galactic Dynamics*. Princeton Series in Astrophysics. Princeton University Press, 2 edition, 2008.
- [34] W. F. Vinen and J. J. Niemela. Quantum turbulence. *J. Low Temp. Phys.*, 128(5):167–231, 2002.
- [35] Carlo F. Barenghi, Russell J. Donnelly, and W. F. Vinen. *Quantized Vortex Dynamics and Superfluid Turbulence*, volume 571 of *Lecture Notes in Physics*. Springer-Verlag, 2001.
- [36] Marios C. Tsatsos, Pedro E. S. Tavares, André Cidrim, Amilson R. Fritsch, Mônica A. Caracanhas, F. Ednilson A. dos Santos, Carlo F. Barenghi, and Vanderlei S. Bagnato. Quantum turbulence in trapped atomic Bose-Einstein condensates. *Phys. Rep.*, 622:1–52, 2016.
- [37] S. Dyachenko, A. C. Newell, A. Pushkarev, and V. E. Zakharov. Optical turbulence: weak turbulence, condensates and collapsing filaments in the nonlinear Schrödinger equation. *Phys. D*, 57(1):96–160, 1992.
- [38] A. Picozzi, J. Garnier, T. Hansson, P. Suret, S. Randoux, G. Millot, and D. N. Christodoulides. Optical wave turbulence: Towards a unified nonequilibrium thermodynamic formulation of statistical nonlinear optics. *Phys. Rep.*, 542(1):1–132, 2014.
- [39] Catherine Sulem and Pierre-Louis Sulem. *The Nonlinear Schrödinger Equation: Self-Focusing and Wave Collapse*, volume 139 of *Applied Mathematical Sciences*. Springer-Verlag, New York, 1999.
- [40] Victor S. L’vov and Sergey Nazarenko. Weak turbulence of Kelvin waves in superfluid He. *Low Temp. Phys.*, 36(8-9):785–791, 2010.

- [41] Yeontaek Choi, Yuri V. Lvov, and Sergey Nazarenko. Probability densities and preservation of randomness in wave turbulence. *Phys. Lett. A*, 332(3-4):230–238, 2004.
- [42] Yeontaek Choi, Yuri V. Lvov, and Sergey Nazarenko. Joint statistics of amplitudes and phases in wave turbulence. *Phys. D*, 201(1-2):121–149, 2005.
- [43] Yeontaek Choi, Yuri V. Lvov, and Sergey Nazarenko. Wave turbulence. In *Recent developments in fluid dynamics*, page 225, Kepala, India, 2004. Transworld Research Network.
- [44] D. V. Semikoz and I. I. Tkachev. Kinetics of Bose condensation. *Phys. Rev. Lett.*, 74(16):3093–3097, 1995.
- [45] D. V. Semikoz and I. I. Tkachev. Condensation of bosons in the kinetic regime. *Phys. Rev. D*, 55(2):489–502, 1997.
- [46] S. Galtier, S. V. Nazarenko, Alan C. Newell, and A. Pouquet. A weak turbulence theory for incompressible magnetohydrodynamics. *J. Plasma Phys.*, 63(5):447–488, 2000.
- [47] Ragnar Fjørtoft. On the changes in the spectral distribution of kinetic energy for twodimensional, nondivergent flow. *Tellus*, 5(3):225–230, 1953.
- [48] Yuri Lvov, Sergey Nazarenko, and Robert West. Wave turbulence in Bose-Einstein condensates. *Phys. D*, 184(1-4):333–351, 2003.
- [49] A.N. Kolmogorov. The local structure of turbulence in incompressible viscous fluid for very large Reynolds numbers. *Proc. R. Soc. Lond. A*, 434:9–13, 1991.
- [50] Colm Connaughton, Sergey Nazarenko, and Alan C. Newell. Dimensional analysis and weak turbulence. *Phys. D*, 184(1-4):86–97, 2003.
- [51] Davide Proment, Miguel Onorato, Pietro Asinari, and Sergey Nazarenko. Warm cascade states in a forced-dissipated Boltzmann gas of hard spheres. *Phys. D*, 241(5):600–615, 2012.
- [52] Colm Connaughton and Rachel McAdams. Mixed flux-equipartition solutions of a diffusion model of nonlinear cascades. *Europhys. Lett. EPL*, 95(2):24005, 2011.
- [53] Colm Connaughton and Sergey Nazarenko. Warm cascades and anomalous scaling in a diffusion model of turbulence. *Phys. Rev. Lett.*, 92(4):044501, 2004.
- [54] Sergey Nazarenko. Differential approximation for Kelvin wave turbulence. *JETP Lett.*, 83(5):198–200, 2006.
- [55] G. Boffetta, A. Celani, D. Dezzani, J. Laurie, and S. Nazarenko. Modeling Kelvin wave cascades in superfluid helium. *J. Low Temp. Phys.*, 156(3-6):193–214, 2009.
- [56] V. S. L’vov and S. Nazarenko. Differential model for 2D turbulence. *JETP Lett.*, 83(12):541–545, 2006.
- [57] V. N. Grebenev, S. B. Medvedev, S. V. Nazarenko, and B. V. Semisalov. Steady states in dual-cascade wave turbulence. *arXiv:2003.04613*.
- [58] Uriel Frisch, Susan Kurien, Rahul Pandit, Walter Pauls, Samriddhi Sankar Ray, Achim Wirth, and Jian-Zhou Zhu. Hyperviscosity, Galerkin truncation, and bottlenecks in turbulence. *Phys. Rev. Lett.*, 101(14):144501, 2008.
- [59] Victor S. L’vov, Sergei V. Nazarenko, and Oleksii Rudenko. Bottleneck crossover between classical and quantum superfluid turbulence. *Phys. Rev. B*, 76(2):024520, 2007.
- [60] Sergei V. Nazarenko and Alexander A. Schekochihin. Critical balance in magnetohydrodynamic, rotating and stratified turbulence: towards a universal scaling conjecture. *J. of Fluid Mech.*, 677:134–153, 2011.
- [61] Argelia Bernal and F Siddhartha Guzmán. Scalar field dark matter: Head-on interaction between two structures. *Phys. Rev. D*, 74(10):103002, 2006.
- [62] Bodo Schwabe, Jens C. Niemeyer, and Jan F. Engels. Simulations of solitonic core mergers in ultralight axion dark matter cosmologies. *Phys. Rev. D*, 94(4):043513, 2016.
- [63] Mustafa A. Amin and Philip Mocz. Formation, gravitational clustering, and interactions of nonrelativistic solitons in an expanding universe. *Phys. Rev. D*, 100(6):063507, 2019.
- [64] F. Siddhartha Guzmán and L. Arturo Ureña-López. Evolution of the Schrödinger-Newton system for a self-gravitating scalar field. *Phys. Rev. D*, 69(12):124033, 2004.
- [65] F. Siddhartha Guzmán and L. Arturo Ureña-López. Gravitational cooling of self-gravitating Bose condensates. *Astrophys. J.*, 645(2):814–819, 2006.